Orbital-Selective Spin-Orbit Mott Insulator in Fractional Valence Iridate $La_3Ir_3O_{11}$

Kai Wang,[1,2,*] Jun Yang,[3] Chaoyang Kang,[4] Weikang Wu,[5] Wenka Zhu,[6]
Jianzhou Zhao,[7,†] Yaomin Dai,[8,‡] and Bing Xu[9,10,§]

[1]*School of Physics and Electronics, Henan University, Kaifeng 475004, China*

[2]*Institute of Quantum Materials and Physics, Henan Academy of Sciences, Zhengzhou 450046, China*

[3]*Department of Materials Science and Engineering, Westlake University, Hangzhou, Zhejiang, China*

[4]*School of Future Technology, Henan University, Zhengzhou 450046, China*

[5]*Key Laboratory for Liquid-Solid Structural Evolution and Processing of Materials, Ministry of Education,
Shandong University, Jinan 250061, China*

[6]*High Magnetic Field Laboratory, Chinese Academy of Sciences, Hefei 230031, China*

[7]*Center for Joint Quantum Studies and Department of Physics, School of Science, Tianjin University,
135 Yaguan Road, Tianjin 300350, China*

[8]*National Laboratory of Solid State Microstructures and Department of Physics, Nanjing University, Nanjing 210093, China*

[9]*Beijing National Laboratory for Condensed Matter Physics, Institute of Physics, Chinese Academy of Sciences,
P.O. Box 603, Beijing 100190, China*

[10]*School of Physical Sciences, University of Chinese Academy of Sciences, Beijing 100049, China*

The combination of strong spin-orbit coupling and Coulomb interactions makes the $5d$ iridates a unique platform for realizing novel correlated electronic states. Here, utilizing infrared spectroscopy, we demonstrate that a robust Mott insulating state persists in the $1/3$-hole self-doped system $La_3Ir_3O_{11}$, evidenced by the collapse of the Drude response and the emergence of sharp excitations across the Mott gap. Our theoretical calculations reveal that the insulating behavior arises from the cooperative interplay of structural distortions, spin-orbit coupling, and Coulomb interactions. Specifically, octahedral distortion and Ir-Ir dimerization split the t_{2g} orbitals, driving the $J_{eff} = 1/2$ bands toward half filling while keeping the $J_{eff} = 3/2$ bands away from it. Consequently, electron correlations induce an orbital-selective Mott transition in the $J_{eff} = 1/2$ bands, whereas a band-insulating gap develops in the $J_{eff} = 3/2$ bands, thereby stabilizing the unconventional insulating state in $La_3Ir_3O_{11}$. These findings provide new insights into the design and understanding of the insulating ground state of spin-orbit-coupled iridates.

Mott insulators, in which insulating behavior arises from strong electron-electron interactions rather than band filling, have been a cornerstone of modern condensed matter physics since their theoretical prediction [1]. They challenge the conventional band theory, as the insulating gap emerges from the Coulomb repulsion U dominating over the kinetic energy W, leading to localized electrons. Doped Mott insulators, most notably the high-T_c cuprates, have profoundly revolutionized our understanding of quantum materials by hosting intertwined orders, pseudogaps, and unconventional superconductivity [2,3]. In $5d$ transition metal oxides such as iridates, strong spin-orbit coupling (SOC) introduces a new dimension to Mott physics. In compounds like Sr_2IrO_4, the interplay between SOC and Coulomb interactions splits the t_{2g} orbitals into spin-orbit-entangled $J_{eff} = 1/2$ and $J_{eff} = 3/2$ states, giving rise to a spin-orbit Mott insulator within the half filled $J_{eff} = 1/2$ band [4–7]. Analogous to cuprates, tuning this Mott state via chemical doping [8–11], strain [12–14], and dimensionality [15,16] has revealed a rich set of emergent correlated phenomena, including novel charge and magnetic order [17–25], pseudogap features [26–28], and possible unconventional superconductivity [29,30].

A critical question underlying these studies is whether a Mott insulating state can survive away from half filling. In conventional single-band Mott systems, as well as in the $J_{eff} = 1/2$ Mott insulators, even weak doping rapidly suppresses the Mott gap and drives the system into a correlated metallic state [1–3,8–11]. In multiorbital systems, additional orbital degrees of freedom enable more intricate correlation effects, such as orbital-selective Mott physics, as extensively discussed in iron-based superconductors and ruthenates [31–38]. Nevertheless, deviations from $3d^5$ or $4d^5$ fillings in these systems typically lead to Hund's metallic behavior. Consequently, stabilizing a correlated

---

*Contact author: kai.wang@henu.edu.cn

†Contact author: jzzhao@tju.edu.cn

‡Contact author: ymdai@nju.edu.cn

§Contact author: bingxu@iphy.ac.cn

insulating state at noninteger filling remains highly non-trivial. Beyond orbital degrees of freedom, structural effects provide an alternative route to reshaping the electronic state in iridates. For example, lattice distortions of the IrO_6 octahedra can lift orbital degeneracies and renormalize bandwidths, while Ir-Ir dimerization induces strong bonding-antibonding splitting that reconstructs the low-energy electronic structure [39–52]. Their interplay with strong spin-orbit coupling and electron correlations creates a highly entangled landscape in which insulating states may persist even at fractional fillings.

In this context, the geometrically frustrated iridate $La_3Ir_3O_{11}$ provides a particularly compelling platform. As shown in Fig. 3(g), it crystallizes in a cubic structure (space group $Pn\bar{3}$), composed of a three-dimensional network of Ir_2O_{10} dimers formed by pairs of edge-sharing IrO_6 octahedra. Importantly, all Ir ions are crystallographically equivalent and carry a uniform fractional valence of $Ir^{4.33+}$ (corresponding to a $5d^{4.67}$ configuration) rather than a mixture of Ir^{4+} and Ir^{5+} states [54–56]. This places $La_3Ir_3O_{11}$ effectively at $1/3$ hole doping relative to a $5d^5$ spin-orbit Mott insulator, a regime where metallic behavior would typically be expected. Surprisingly, however, $La_3Ir_3O_{11}$ shows no evidence of coherent quasiparticle excitations but instead remains insulating [54], posing a direct challenge to conventional understanding of doped Mott systems.

In this Letter, we investigate the origin of this unconventional insulating state through optical conductivity measurements combined with first-principles calculations. We show that $La_3Ir_3O_{11}$ hosts a robust correlated insulating state, characterized by the collapse of the Drude response and the emergence of sharp low-energy excitations. Our theoretical analysis reveals that distortions within the Ir_2O_{10} dimers split the t_{2g} manifold in an orbital-selective manner, bringing the $J_{eff} = 1/2$ bands close to half filling while pushing the $J_{eff} = 3/2$ bands away. The resulting coexistence of a Mott gap in the $J_{eff} = 1/2$ bands and a band gap in the $J_{eff} = 3/2$ bands stabilizes a spin-orbit-assisted, orbital-selective insulating state at fractional filling in $La_3Ir_3O_{11}$.

Sample synthesis, experimental methods, and details of Drude-Lorentz analysis and theoretical calculations are provided in Supplemental Material [57].

Figure 1(a) displays the temperature-dependent reflectivity spectra of $La_3Ir_3O_{11}$ up to 0.3 eV. The inset of Fig. 1(a) shows the reflectivity at 300 K for the entire measured spectral range. At room temperature, the reflectivity exhibits a plasma edge below 0.05 eV, accompanied by a prominent bump feature around 0.13 eV. With decreasing temperature, the plasma edge shifts to lower energies and eventually disappears below 50 K, while the bump feature becomes more pronounced. In addition to these gross electronic features, a series of infrared-active phonon modes is present in the far-infrared region, which

becomes sharper and more prominent at lower temperatures because of the reduced electron screening. Similar phenomena are frequently observed in the context of the metal-insulator transition in various correlated materials [68,69]. Overall, the significantly decreased or absent plasma edge, along with the prominent phonon behavior, points toward an insulating nature of electrons at low temperatures.

Figure 1(b) depicts the temperature dependence of the optical conductivity $\sigma_1(\omega)$ of $La_3Ir_3O_{11}$ up to 0.3 eV. The low-energy $\sigma_1(\omega)$ presents a Drude-like peak (labeled as D) with $\sigma_1(\omega \to 0) \simeq 800\ \Omega^{-1}\ cm^{-1}$ at $T = 300$ K. Moving to higher frequencies, there is a broad absorption peak (labeled as α) centered around 0.13 eV, consistent with the observation from the previous reflectivity spectrum. As the temperature decreases, the Drude-like peak gradually loses its spectral weight (SW), with $\sigma_1(\omega \to 0)$ decreasing in correlation with the inverse of the resistivity observed in transport. Meanwhile, the α peak gains more SW while maintaining a relatively unchanged peak position. Below ~ 50 K, the Drude response is entirely quenched, resulting in an optical gap below approximately 0.06 eV. Notably, at low temperatures, a distinct shoulder feature (labeled as M) appears around 0.09 eV. The inset of Fig. 1(b) highlights the temperature evolution of the three features by showing the temperature dependence of $\sigma_1(\omega)$ at their peak positions.

Figure 1(c) shows the temperature-dependent $\sigma_1(\omega)$ up to 1.2 eV. In this range, the spectrum features a double peak structure, denoted as α and β. A direct comparison of $\sigma_1(\omega)$ for $La_3Ir_3O_{11}$ with the $5d^5$ iridates Sr_2IrO_4 [11], $Sr_3Ir_2O_7$ [27], and $SrIrO_3$ [53] is presented in Fig. 1(d), all of which display similar features. In Sr_2IrO_4, as illustrated in Figs. 1(e) and 1(f), the on site Coulomb interaction U can split the half filled $J_{eff} = 1/2$ bands into a lower Hubbard band (LHB) and an upper Hubbard band (UHB), thus opening a Mott gap. In this context, the α peak arises from LHB $\to$ UHB transitions, while the β peak originates from $J_{eff} = 3/2 \to$ UHB excitations [5,6,70]. As shown in Fig. 1(d), both the α and β peak positions (E_α and E_β) decrease systematically from Sr_2IrO_4 to $SrIrO_3$, reflecting increasing bandwidth (W) [15,70], since $\Delta \propto U - aW$, with ΔE_α (0.43 eV) being roughly twice ΔE_β (0.27 eV), as sketched in Figs. 1(f) and 1(g). In $La_3Ir_3O_{11}$, the α and β peaks nearly coincide with those of $SrIrO_3$, implying comparable $J_{eff} = 1/2$ bandwidths. However, unlike the semimetallic $SrIrO_3$, $La_3Ir_3O_{11}$ develops an optical gap, and its α peak is strikingly sharper, indicating low-energy excitations associated with quasi-flat bands stabilized by strong electron correlations. These observations suggest that the α and β features in $La_3Ir_3O_{11}$ share the same underlying physics as in Sr_2IrO_4, as sketched in Figs. 1(f) and 1(h), with the robust Mott correlations underpinning its insulating state in $La_3Ir_3O_{11}$.

The role of Mott correlations is further evident by the SW analysis, quantified by $S(\omega, T) = \int_0^\omega \sigma_1(\omega, T)d\omega$. This analysis allows us to identify the nature of the insulating
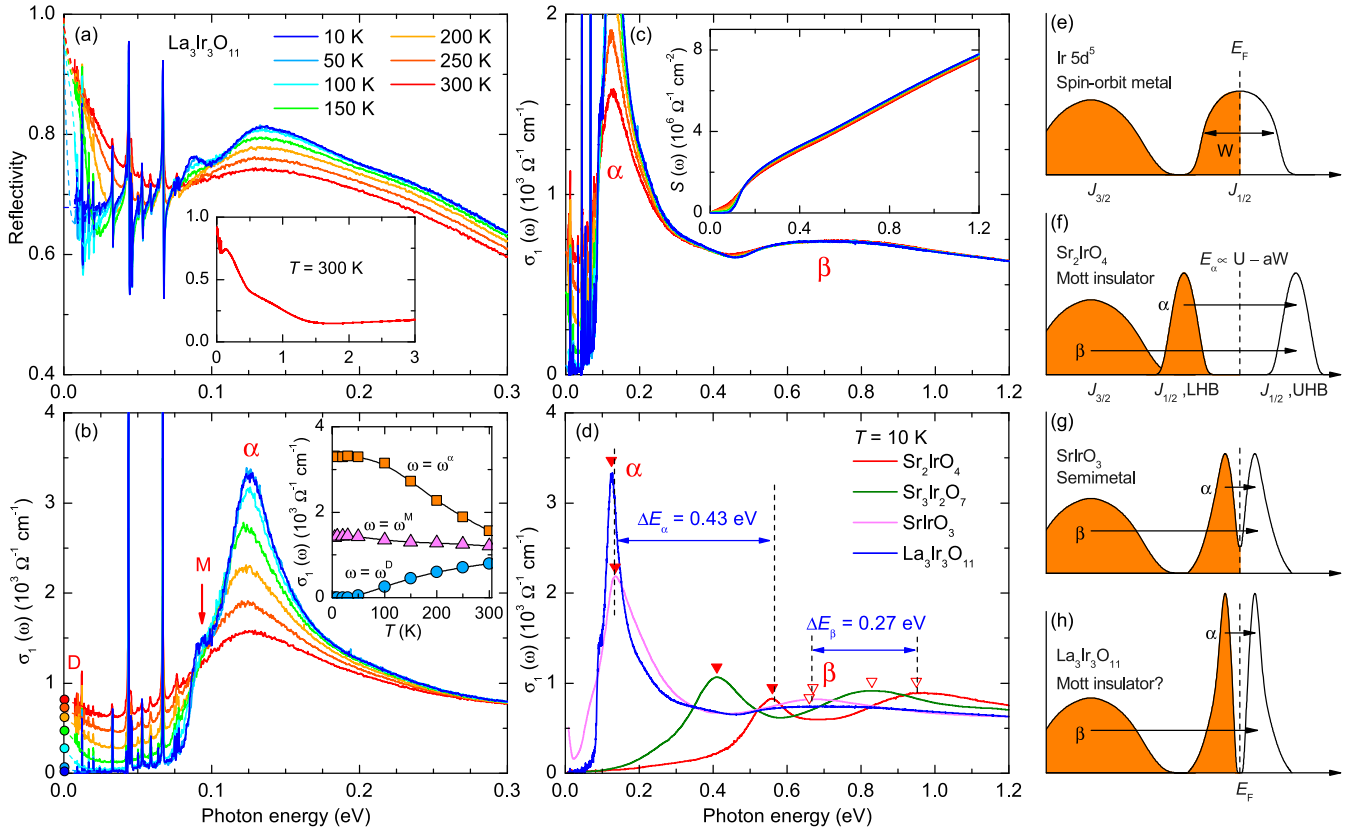
FIG. 1. (a) Temperature-dependent reflectivity $R(\omega)$ of $La_3Ir_3O_{11}$ up to 0.3 eV. The dashed line represents the corresponding low-energy extrapolation. Inset: spectrum up to 3 eV at 300 K. (b) Temperature-dependent optical conductivity up to 0.3 eV. Symbols on the y axis denote dc conductivity values at corresponding temperatures from transport data. (c) Optical conductivity up to 1.2 eV to show the spectral changes at high frequencies. Inset: the energy dependence of spectral weight at several selected temperatures. (d) Comparison of $\sigma_1(\omega)$ between $La_3Ir_3O_{11}$ and the $5d^5$ iridates Sr_2IrO_4 [11], $Sr_3Ir_2O_7$ [27], and $SrIrO_3$ [53] at 10 K. (e)–(h) Diagrams of density of states for different materials.

state, "like band insulator or Mott insulator" [71]. The energy dependence of $S(\omega, T)$ at several representative temperatures is showed in the inset of Fig. 1(c). With decreasing temperature, the free carrier response is completely quenched at low temperatures, while the lost SW does not fully recover within the α peak energy scale. Instead, it redistributes over a broad energy range, extending beyond 1.5 eV, which is comparable with the energy associated with the local on site Coulomb interaction U of Ir $5d$ orbitals [72]. Thus, the observed anomalous SW transfer can be attributed to the "Mottness" of this system in $La_3Ir_3O_{11}$.

To better illustrate the temperature evolution of various components in the $\sigma_1(\omega)$ spectra, we employ the Drude-Lorentz model to fit the data (see details in Supplemental Material [57]). As shown in Fig 2(a), after subtracting the phonon modes, the low-energy $\sigma_1(\omega)$ can be decomposed into three components: the Drude response (D), the shoulder feature (M), and the α excitations. Figures 2(b)–2(d) show the temperature dependence of SW for each component. Obviously, the SW of the M and α components increases with decreasing temperature, while the SW of the Drude

response diminishes. Moreover, the accumulated SW of the M and α excitations exceeds the SW lost by the Drude response, indicating that additional SW is transferred from
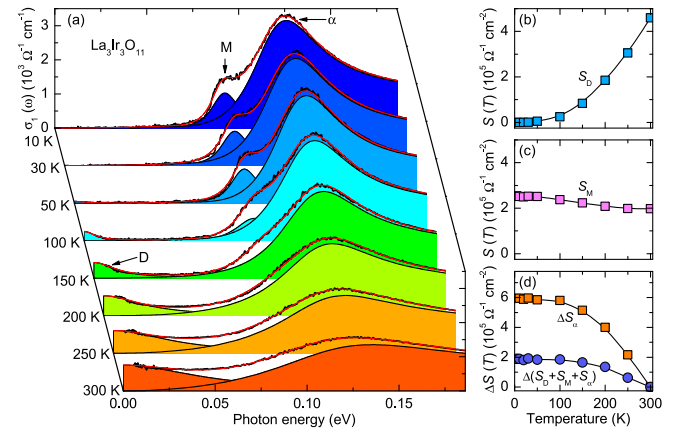

FIG. 2. (a) Drude-Lorentz fits applied to $\sigma_1(\omega)$ spectra. (b)–(d) Temperature dependence of spectral weight for different components. $\Delta S(T) = S(T) - S(300\text{ K})$ represents the difference in spectral weight relative to the value at 300 K.
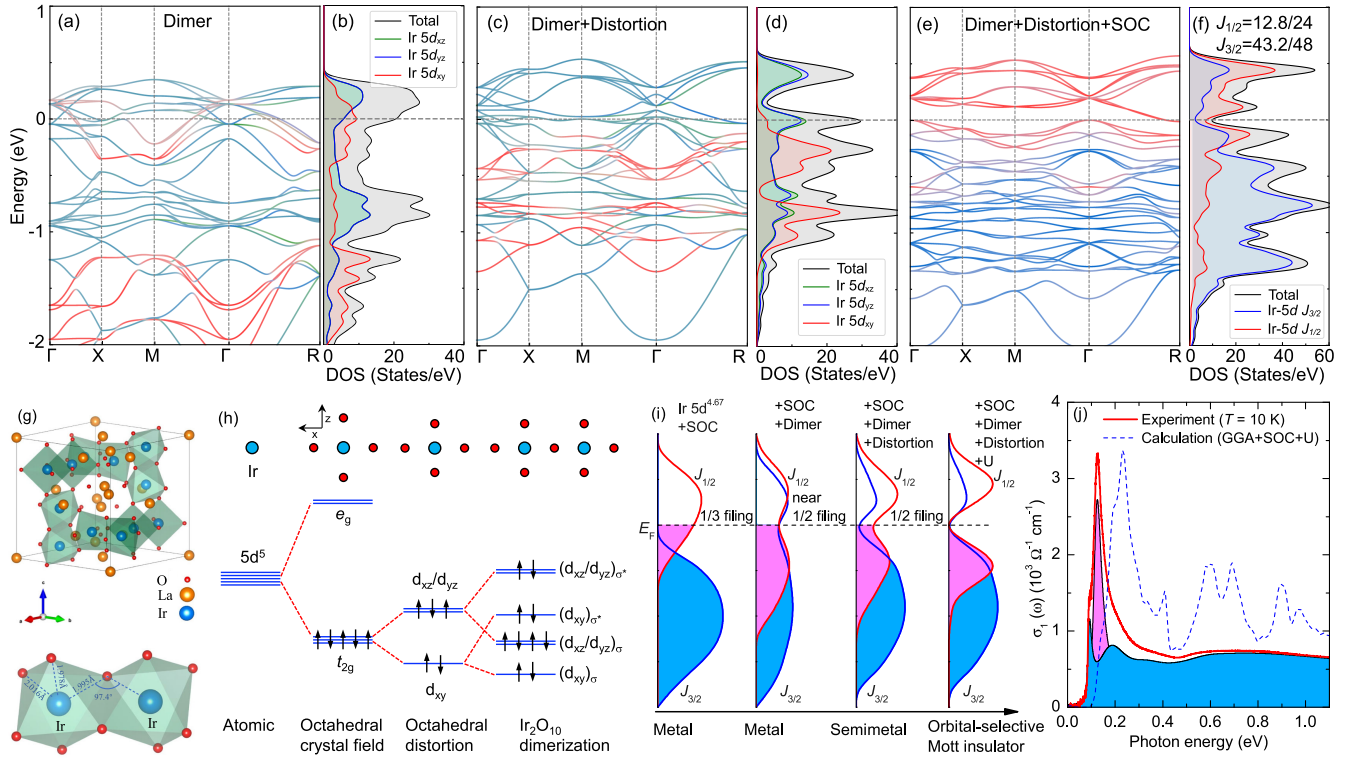
FIG. 3.   Tight-binding band structure and orbital-resolved density of states (DOS) for $La_3Ir_3O_{11}$ with (a),(b) dimerization only, (c), (d) dimerization and octahedral distortion, and (e),(f) dimerization, distortion, and spin-orbit coupling (SOC). (g) Crystal structure of $La_3Ir_3O_{11}$ and the Ir_2O_{10} dimer structure. (h) Orbital-energy-level diagram for the IrO_6 octahedra under various conditions. (i) DOS schematics within the J_{eff} framework for $La_3Ir_3O_{11}$ under the corresponding conditions. (j) Comparison between the experimental and calculated optical conductivity $\sigma_1(\omega)$.

higher energies, which also aligns with our previous analysis.

Based on the above experimental results and discussions, we establish that the insulating state and the sharp α peak arise from the excitations across Mott-Hubbard bands. Nevertheless, two key puzzles immediately arise. First, how can $La_3Ir_3O_{11}$ maintain a robust Mott insulating ground state at a fractional filling of Ir $5d^{4.67}$, which naturally favors a metallic state? Second, what is the origin of the shoulder feature (M) observed within the Mott gap? These issues indicate that the correlated insulating state in $La_3Ir_3O_{11}$ is unconventional and cannot be fully explained by a single-band Mott-Hubbard framework. Regarding the origin of the M mode, several possibilities can be excluded. In-gap states are unlikely, as such excitations typically gain SW from the main Mott excitations (the α peak), as observed in $Sr_2Ir_{1-x}Rh_xO_4$ [11], in clear contradiction with our experimental observations in $La_3Ir_3O_{11}$. A magnetic origin, such as exciton and magnon sideband absorptions observed in rare-earth iridates [73], is also improbable, given the absence of long-range magnetic order in $La_3Ir_3O_{11}$ [54].

To further elucidate the origin of the insulating state and low-energy excitations in $La_3Ir_3O_{11}$, we performed systematic band calculations under various conditions (see Sec. C

of Supplemental Material [57]). These calculations allow us to disentangle the distinct roles of dimerization, octahedral distortion, spin-orbit coupling, and electron correlations, and to clarify how their cooperative interplay stabilizes the observed insulating state. We first examine the structural effects. In the absence of SOC and electron correlations, as shown in Figs. 3(a)–3(d), the system exhibits a metallic electronic structure, with states near the Fermi level dominated by Ir t_{2g} orbitals due to the octahedral crystal-field splitting. The formation of Ir_2O_{10} dimers gives rise to a pronounced bonding-antibonding splitting of the t_{2g} orbitals [Figs. 3(a) and 3(b)], reflecting the molecular-orbital character imposed by the dimerized units. When the experimentally observed octahedral distortion (compressed along the z axis) is included [Figs. 3(c) and 3(d)], the t_{2g} degeneracy is further lifted: the d_{xz}/d_{yz} orbitals are shifted to higher energies and become less occupied, whereas the d_{xy} orbital is pushed to lower energies and becomes more occupied. This progressive orbital reconstruction, driven by crystal-field, octahedral distortions and dimerization, is schematically summarized in Fig. 3(h).

When SOC is explicitly included, the system evolves into a compensated semimetal, featuring hole pockets at the Γ and electron pockets at R, as shown in Figs. 3(e) and 3(f).

Analysis in the $J_{\rm eff}$ basis reveals two consequences promoted by octahedral distortion, as compared in Fig. S6 in Supplemental Material [57]. First, the separation between the $J_{\rm eff} = 1/2$ and $J_{\rm eff} = 3/2$ manifolds is significantly enhanced. Second the $J_{\rm eff} = 1/2$ bands are driven close to half filling (12.8/24 electrons). The nearly half filled condition naturally amplifies the susceptibility of the $J_{\rm eff} = 1/2$ bands to an orbital-selective Mott transition. At the same time, the distortion opens a small semiconducting gap within the $J_{\rm eff} = 3/2$ bands. Within this $J_{\rm eff}$ framework, the electronic evolution of $La_3Ir_3O_{11}$ can be summarized schematically in Fig. 3(i): dimerization establishes the basic bonding-antibonding structure and suppresses the density of states near the Fermi level; octahedral distortion enhances orbital differentiation and drives the $J_{\rm eff} = 1/2$ bands toward half filling; electron correlations then selectively act on this nearly half filled sector to open a Mott gap. Indeed, when correlations are included via generalized gradient approximation with spin-orbit coupling and Hubbard U parameter (GGA + SOC + U) calculations (Fig. S7 in Supplemental Material [57]), the residual density of states at the Fermi level is removed and a global insulating gap opens. The resulting ground state is therefore characterized by a Mott gap in the $J_{\rm eff} = 1/2$ bands coexisting with a band gap in the $J_{\rm eff} = 3/2$ bands, stabilizing the unconventional insulating state in $La_3Ir_3O_{11}$.

This dual-gap electronic structure naturally accounts for the optical response. As shown in Fig. 3(j), the calculated optical conductivity reproduces the main experimental features, albeit with broader peaks and a systematic blueshift due to the underestimation of correlation-induced bandwidth renormalization in density-functional theory with Hubbard U parameter (DFT + U) calculations [70]. Within coexistence of Mott and band gaps, the low-energy optical response of $La_3Ir_3O_{11}$ can be qualitatively decomposed into two components: (i) Mott-gap excitations of the $J_{\rm eff} = 1/2$ bands, which give rise to the sharp α peak (magenta shading), and (ii) interband excitations across the gap in the $J_{\rm eff} = 3/2$ bands, responsible for the shoulder (M mode) and the broad background beneath the α peak (light-blue shading).

Finally, we discuss the implications of our Letter. At the materials level, the relatively large bandwidth in $La_3Ir_3O_{11}$ places the ratio U/W close to the critical value for a Mott transition, making the insulating state highly sensitive to external parameters such as temperature. As a result, pronounced SW transfer between the Mott gap and Drude-like excitations is observed. In addition, variations in sample growth conditions can effectively tune lattice distortion or carrier filling, potentially driving the system back into a semimetallic state, as reported in previous studies in $La_3Ir_3O_{11}$ [55]. Such high tunability establishes $La_3Ir_3O_{11}$ as a promising platform for controlling correlated quantum phases. More fundamentally, our findings extend the paradigm of Mott insulating behavior in spin-orbit-coupled systems beyond half filled single-band models. We demonstrate that orbital-selective correlations can stabilize a Mott-insulating $J_{\rm eff} = 1/2$ band coexisting with a band-insulating $J_{\rm eff} = 3/2$ background, even at fractional valence. The cooperative interplay of structural distortions, SOC, and multiorbital correlations thus provides a general route to unconventional insulating states. In this context, our Letter is consistent with recent theoretical proposals of orbital-selective Mott physics in spin-orbit-coupled multiorbital systems [74,75] and suggests new strategies for engineering novel quantum phases in correlated materials.

Data availability—The data that support the findings of this article are not publicly available. The data are available from the authors upon reasonable request.

[1] M. Imada, A. Fujimori, and Y. Tokura, Metal-insulator transitions, Rev. Mod. Phys. **70**, 1039 (1998).

[2] E. Dagotto, Correlated electrons in high-temperature superconductors, Rev. Mod. Phys. **66**, 763 (1994).

[3] P. A. Lee, N. Nagaosa, and X.-G. Wen, Doping a Mott insulator: Physics of high-temperature superconductivity, Rev. Mod. Phys. **78**, 17 (2006).

[4] B. J. Kim, H. Ohsumi, T. Komesu, S. Sakai, T. Morita, H. Takagi, and T. Arima, Phase-sensitive observation of a spin-orbital Mott state in Sr_2IrO_4, Science **323**, 1329 (2009).

[5] B. J. Kim, H. Jin, S. J. Moon, J.-Y. Kim, B.-G. Park, C. S. Leem, J. Yu, T. W. Noh, C. Kim, S.-J. Oh, J.-H. Park, V. Durairaj, G. Cao, and E. Rotenberg, Novel $J_{\rm eff} = 1/2$ Mott state induced by relativistic spin-orbit coupling in Sr_2IrO_4, Phys. Rev. Lett. **101**, 076402 (2008).

[6] S. J. Moon, H. Jin, W. S. Choi, J. S. Lee, S. S. A. Seo, J. Yu, G. Cao, T. W. Noh, and Y. S. Lee, Temperature dependence of the electronic structure of the $J_{\rm eff} = \frac{1}{2}$ Mott insulator Sr_2IrO_4 studied by optical spectroscopy, Phys. Rev. B **80**, 195110 (2009).

[7] G. Jackeli and G. Khaliullin, Mott insulators in the strong spin-orbit coupling limit: From Heisenberg to a quantum compass and Kitaev models, Phys. Rev. Lett. **102**, 017205 (2009).

[8] T. F. Qi, O. B. Korneta, L. Li, K. Butrouna, V. S. Cao, X. Wan, P. Schlottmann, R. K. Kaul, and G. Cao, Spin-orbit tuned metal-insulator transitions in single-crystal $Sr_2Ir_{1-x}Rh_xO_4$ ($0 \leq x \leq 1$), Phys. Rev. B **86**, 125105 (2012).

[9] J. S. Lee, Y. Krockenberger, K. S. Takahashi, M. Kawasaki, and Y. Tokura, Insulator-metal transition driven by change of doping and spin-orbit interaction in Sr_2IrO_4, Phys. Rev. B **85**, 035101 (2012).

[10] Y. Cao, Q. Wang, J. A. Waugh, T. J. Reber, H. Li, X. Zhou, S. Parham, S.-R. Park, N. C. Plumb, E. Rotenberg, A. Bostwick, J. D. Denlinger, T. Qi, M. A. Hermele, G. Cao, and D. S. Dessau, Hallmarks of the Mott-metal crossover in the hole-doped pseudospin-1/2 Mott insulator Sr_2IrO_4, Nat. Commun. **7**, 11367 (2016).

[11] B. Xu, P. Marsik, E. Sheveleva, F. Lyzwa, A. Louat, V. Brouet, D. Munzar, and C. Bernhard, Optical signature of a crossover from Mott- to Slater-type gap in $Sr_2Ir_{1-x}Rh_xO_4$, Phys. Rev. Lett. **124**, 027402 (2020).

[12] E. Paris, Y. Tseng, E. M. Pärschke, W. Zhang, M. H. Upton, A. Efimenko, K. Rolfs, D. E. McNally, L. Maurel, M. Naamneh, M. Caputo, V. N. Strocov, Z. Wang, D. Casa, C. W. Schneider, E. Pomjakushina, K. Wohlfeld, M. Radovic, and T. Schmitt, Strain engineering of the charge and spin-orbital interactions in Sr_2IrO_4, Proc. Natl. Acad. Sci. U.S.A. **117**, 24764 (2020).

[13] S. Shrestha, M. Krautloher, M. Zhu, J. Kim, J. Hwang, J. Kim, J.-W. Kim, B. Keimer, and A. Seo, Emergent inter-layer magnetic order via strain-induced orthorhombic distortion in the $5d$ Mott insulator Sr_2IrO_4, Phys. Rev. B **105**, L100404 (2022).

[14] L. Engström, C.-C. Liu, W. Witczak-Krempa, and T. Pereg-Barnea, Strain-induced superconductivity in Sr_2IrO_4, Phys. Rev. B **108**, 014508 (2023).

[15] S. J. Moon, H. Jin, K. W. Kim, W. S. Choi, Y. S. Lee, J. Yu, G. Cao, A. Sumi, H. Funakubo, C. Bernhard, and T. W. Noh, Dimensionality-controlled insulator-metal transition and correlated metallic state in $5d$ transition metal oxides $Sr_{n+1}Ir_nO_{3n+1}$ ($n = 1$, 2, and ∞), Phys. Rev. Lett. **101**, 226402 (2008).

[16] Q. Wang, Y. Cao, J. A. Waugh, S. R. Park, T. F. Qi, O. B. Korneta, G. Cao, and D. S. Dessau, Dimensionality-controlled Mott transition and correlation effects in single-layer and bilayer perovskite iridates, Phys. Rev. B **87**, 245109 (2013).

[17] Y. K. Kim, O. Krupin, J. Denlinger, A. Bostwick, E. Rotenberg, Q. Zhao, J. Mitchell, J. Allen, and B. Kim, Fermi arcs in a doped pseudospin-1/2 Heisenberg antiferromagnet, Science **345**, 187 (2014).

[18] J. Kim, M. Daghofer, A. Said, T. Gog, J. Van den Brink, G. Khaliullin, and B. Kim, Excitonic quasiparticles in a spin-orbit Mott insulator, Nat. Commun. **5**, 4453 (2014).

[19] L. Zhao, D. Torchinsky, H. Chu, V. Ivanov, R. Lifshitz, R. Flint, T. Qi, G. Cao, and D. Hsieh, Evidence of an odd-parity hidden order in a spin-orbit coupled correlated iridate, Nat. Phys. **12**, 32 (2016).

[20] S. Zhou, K. Jiang, H. Chen, and Z. Wang, Correlation effects and hidden spin-orbit entangled electronic order in parent and electron-doped iridates Sr_2IrO_4, Phys. Rev. X **7**, 041018 (2017).

[21] J. Jeong, Y. Sidis, A. Louat, V. Brouet, and P. Bourges, Time-reversal symmetry breaking hidden order in $Sr_2(Ir, Rh)O_4$, Nat. Commun. **8**, 15119 (2017).

[22] K. Wang, N. Bachar, J. Teyssier, W. Luo, C. W. Rischau, G. Scheerer, A. de la Torre, R. S. Perry, F. Baumberger, and D. van der Marel, Mott transition and collective charge pinning in electron doped Sr_2IrO_4, Phys. Rev. B **98**, 045107 (2018).

[23] G. Cao, J. Terzic, H. D. Zhao, H. Zheng, L. E. De Long, and P. S. Riseborough, Electrical control of structural and physical properties via strong spin-orbit interactions in Sr_2IrO_4, Phys. Rev. Lett. **120**, 017201 (2018).

[24] H. Murayama, K. Ishida, R. Kurihara, T. Ono, Y. Sato, Y. Kasahara, H. Watanabe, Y. Yanase, G. Cao, Y. Mizukami, T. Shibauchi, Y. Matsuda, and S. Kasahara, Bond directional anapole order in a spin-orbit coupled Mott insulator $Sr_2(Ir_{1-x}Rh_x)O_4$, Phys. Rev. X **11**, 011021 (2021).

[25] H. Kim, J. K. Kim, J. Kwon, J. Kim, H. W. J. Kim, S. Ha, K. Kim, W. Lee, J. Kim, G. Y. Cho, H. Heo, J. Jang, C. J. Sahle, A. Longo, J. Strempfer, G. Fabbris, Y. Choi, D. Haskel, J. Kim, J. W. Kim, and B. J. Kim, Quantum spin nematic phase in a square-lattice iridate, Nature (London) **625**, 264 (2024).

[26] I. Battisti, K. M. Bastiaans, V. Fedoseev, A. de la Torre, N. Iliopoulos, A. Tamai, E. C. Hunter, R. S. Perry, J. Zaanen, F. Baumberger, and M. P. Allan, Universality of pseudogap and emergent order in lightly doped Mott insulators, Nat. Phys. **13**, 21 (2017).

[27] J. H. Seo, G. H. Ahn, S. J. Song, X. Chen, S. D. Wilson, and S. J. Moon, Infrared probe of pseudogap in electron-doped Sr_2IrO_4, Sci. Rep. **7**, 10494 (2017).

[28] A. Louat, B. Lenz, S. Biermann, C. Martins, F. Bertran, P. Le Fèvre, J. E. Rault, F. Bert, and V. Brouet, ARPES study of orbital character, symmetry breaking, and pseudogaps in doped and pure Sr_2IrO_4, Phys. Rev. B **100**, 205135 (2019).

[29] F. Wang and T. Senthil, Twisted Hubbard model for Sr_2IrO_4: Magnetism and possible high temperature superconductivity, Phys. Rev. Lett. **106**, 136402 (2011).

[30] Y. J. Yan, M. Q. Ren, H. C. Xu, B. P. Xie, R. Tao, H. Y. Choi, N. Lee, Y. J. Choi, T. Zhang, and D. L. Feng, Electron-doped Sr_2IrO_4: An analogue of hole-doped cuprate superconductors demonstrated by scanning tunneling microscopy, Phys. Rev. X **5**, 041018 (2015).

[31] L. de'Medici, A. Georges, and S. Biermann, Orbital-selective Mott transition in multiband systems: Slave-spin representation and dynamical mean-field theory, Phys. Rev. B **72**, 205124 (2005).

[32] L. de'Medici, S. R. Hassan, M. Capone, and X. Dai, Orbital-selective Mott transition out of band degeneracy lifting, Phys. Rev. Lett. **102**, 126401 (2009).

[33] L. de'Medici, G. Giovannetti, and M. Capone, Selective Mott physics as a key to iron superconductors, Phys. Rev. Lett. **112**, 177001 (2014).

[34] R. Yu and Q. Si, Orbital-selective Mott phase in multiorbital models for alkaline iron selenides $K_{1-x}Fe_{2-y}Se_2$, Phys. Rev. Lett. **110**, 146402 (2013).

[35] R. Yu and Q. Si, Orbital-selective Mott phase in multiorbital models for iron pnictides and chalcogenides, Phys. Rev. B **96,** 125110 (2017).

[36] M. Kim, S. Choi, W. H. Brito, and G. Kotliar, Orbital-selective Mott transition effects and nontrivial topology of iron chalcogenide, Phys. Rev. Lett. **132,** 136504 (2024).

[37] S.-C. Wang, H.-B. Yang, A. K. P. Sekharan, S. Souma, H. Matsui, T. Sato, T. Takahashi, C. Lu, J. Zhang, R. Jin, D. Mandrus, E. W. Plummer, Z. Wang, and H. Ding, Fermi surface topology of $Ca_{1.5}Sr_{0.5}RuO_4$ determined by angle-resolved photoelectron spectroscopy, Phys. Rev. Lett. **93,** 177007 (2004).

[38] M. Neupane, P. Richard, Z.-H. Pan, Y.-M. Xu, R. Jin, D. Mandrus, X. Dai, Z. Fang, Z. Wang, and H. Ding, Observation of a novel orbital selective Mott transition in $Ca_{1.8}Sr_{0.2}RuO_4$, Phys. Rev. Lett. **103,** 097001 (2009).

[39] G. Cao and P. Schlottmann, The challenge of spin-orbit-tuned ground states in iridates: A key issues review, Rep. Prog. Phys. **81,** 042502 (2018).

[40] I. I. Mazin, H. O. Jeschke, K. Foyevtsova, R. Valentí, and D. I. Khomskii, Na_2IrO_3 as a molecular orbital crystal, Phys. Rev. Lett. **109,** 197201 (2012).

[41] X. Liu, V. M. Katukuri, L. Hozoi, W.-G. Yin, M. P. M. Dean, M. H. Upton, J. Kim, D. Casa, A. Said, T. Gog, T. F. Qi, G. Cao, A. M. Tsvelik, J. van den Brink, and J. P. Hill, Testing the validity of the strong spin-orbit-coupling limit for octahedrally coordinated iridate compounds in a model system Sr_3CuIrO_6, Phys. Rev. Lett. **109,** 157401 (2012).

[42] H. Gretarsson, J. P. Clancy, X. Liu, J. P. Hill, E. Bozin, Y. Singh, S. Manni, P. Gegenwart, J. Kim, A. H. Said, D. Casa, T. Gog, M. H. Upton, H.-S. Kim, J. Yu, V. M. Katukuri, L. Hozoi, J. van den Brink, and Y.-J. Kim, Crystal-field splitting and correlation effect on the electronic structure of A_2IrO_3, Phys. Rev. Lett. **110,** 076402 (2013).

[43] T. Dey, R. Kumar, A. V. Mahajan, S. D. Kaushik, and V. Siruguri, Unconventional magnetism in the spin-orbit-driven Mott insulators $Ba_3MIr_2O_9$ (M = Sc, Y), Phys. Rev. B **89,** 205101 (2014).

[44] J. Terzic, J. C. Wang, F. Ye, W. H. Song, S. J. Yuan, S. Aswartham, L. E. DeLong, S. V. Streltsov, D. I. Khomskii, and G. Cao, Coexisting charge and magnetic orders in the dimer-chain iridate $Ba_5AlIr_2o_{11}$, Phys. Rev. B **91,** 235147 (2015).

[45] V. Hermann, M. Altmeyer, J. Ebad-Allah, F. Freund, A. Jesche, A. A. Tsirlin, M. Hanfland, P. Gegenwart, I. I. Mazin, D. I. Khomskii, R. Valentí, and C. A. Kuntscher, Competition between spin-orbit coupling, magnetism, and dimerization in the honeycomb iridates: $\alpha - Li_2IrO_3$ under pressure, Phys. Rev. B **97,** 020104 (2018).

[46] M. Ye, H.-S. Kim, J.-W. Kim, C.-J. Won, K. Haule, D. Vanderbilt, S.-W. Cheong, and G. Blumberg, Covalency-driven collapse of strong spin-orbit coupling in face-sharing iridium octahedra, Phys. Rev. B **98,** 201105 (2018).

[47] Y. Wang, R. Wang, J. Kim, M. H. Upton, D. Casa, T. Gog, G. Cao, G. Kotliar, M. P. M. Dean, and X. Liu, Direct detection of dimer orbitals in $Ba_5AlIr_2O_{11}$, Phys. Rev. Lett. **122,** 106401 (2019).

[48] H. Zhao, F. Ye, H. Zheng, B. Hu, Y. Ni, Y. Zhang, I. Kimchi, and G. Cao, Ground state in the novel dimer iridate $Ba_{13}Ir_6O_{30}$ with $Ir^{6+}(5d^3)$ ions, Phys. Rev. B **100,** 064418 (2019).

[49] M. S. Khan, A. Bandyopadhyay, A. Nag, V. Kumar, A. V. Mahajan, and S. Ray, Magnetic ground state of the distorted $6H$ perovskite $Ba_3CdIr_2O_9$, Phys. Rev. B **100,** 064423 (2019).

[50] J. Jeong, B. Lenz, A. Gukasov, X. Fabrèges, A. Sazonov, V. Hutanu, A. Louat, D. Bounoua, C. Martins, S. Biermann, V. Brouet, Y. Sidis, and P. Bourges, Magnetization density distribution of Sr_2IrO_4: Deviation from a local $J_{eff} = 1/2$ picture, Phys. Rev. Lett. **125,** 097202 (2020).

[51] S. Kumar, S. K. Panda, M. M. Patidar, S. K. Ojha, P. Mandal, G. Das, J. W. Freeland, V. Ganesan, P. J. Baker, and S. Middey, Spin-liquid behavior of the three-dimensional magnetic system $Ba_3NiIr_2O_9$ with $S = 1$, Phys. Rev. B **103,** 184405 (2021).

[52] C. Lane, Y. Zhang, J. W. Furness, R. S. Markiewicz, B. Barbiellini, J. Sun, and A. Bansil, First-principles calculation of spin and orbital contributions to magnetically ordered moments in Sr_2IrO_4, Phys. Rev. B **101,** 155110 (2020).

[53] J. Fujioka, T. Okawa, M. Masuko, A. Yamamoto, and Y. Tokura, Charge dynamics and metal-insulator transition in perovskite $SrIr_{1-x}Sn_xO_3$, J. Phys. Soc. Jpn. **87,** 123706 (2018).

[54] J. Yang, J. R. Wang, W. L. Zhen, L. Ma, L. S. Ling, W. Tong, C. J. Zhang, L. Pi, and W. K. Zhu, Frustration-induced non-Curie-Weiss paramagnetism in $La_3Ir_3O_{11}$: A fractional valence state iridate, Phys. Rev. B **100,** 205107 (2019).

[55] T. Aoyama, K. Emi, C. Tabata, Y. Nambu, H. Nakao, T. Yamauchi, and K. Ohgushi, A semimetallic state in $La_3Ir_3O_{11}$ with the $KSbO_3$ structure, J. Phys. Soc. Jpn. **88,** 093706 (2019).

[56] F. Abraham, J. Trehoux, D. Thomas, and F. Wagner, Propriétés électriques, magnétiques et de résonance Mössbauer de $La_3Ir_3O_{11}$, J. Less Common Met. **84,** 245 (1982).

[57] See Supplemental Material at http://link.aps.org/supplemental/10.1103/24vx-xm5d for the details of sample synthesis, experimental methods, and details of Drude-Lorentz analysis and theoretical calculations, which includes Refs. [58–67].

[58] C. C. Homes, M. Reedyk, D. A. Cradles, and T. Timusk, Technique for measuring the reflectance of irregular, sub-millimeter-sized samples, Appl. Opt. **32,** 2976 (1993).

[59] M. Dressel and G. Grüner, *Electrodynamics of Solids* (Cambridge University Press, Cambridge, England, 2002).

[60] G. Kresse and J. Furthmüller, Efficient iterative schemes for *ab initio* total-energy calculations using a plane-wave basis set, Phys. Rev. B **54,** 11169 (1996).

[61] G. Kresse and J. Furthmüller, Efficiency of *ab-initio* total energy calculations for metals and semiconductors using a plane-wave basis set, Comput. Mater. Sci. **6,** 15 (1996).

[62] G. Kresse and D. Joubert, From ultrasoft pseudopotentials to the projector augmented-wave method, Phys. Rev. B **59,** 1758 (1999).

[63] P. E. Blöchl, Projector augmented-wave method, Phys. Rev. B **50,** 17953 (1994).

[64] J. P. Perdew, K. Burke, and M. Ernzerhof, Generalized gradient approximation made simple, Phys. Rev. Lett. **77,** 3865 (1996).

[65] S. L. Dudarev, G. A. Botton, S. Y. Savrasov, C. J. Humphreys, and A. P. Sutton, Electron-energy-loss spectra and the structural stability of nickel oxide: An LSDA + U study, Phys. Rev. B **57**, 1505 (1998).

[66] N. Marzari, A. A. Mostofi, J. R. Yates, I. Souza, and D. Vanderbilt, Maximally localized Wannier functions: Theory and applications, Rev. Mod. Phys. **84**, 1419 (2012).

[67] A. Marrazzo, S. Beck, E. R. Margine, N. Marzari, A. A. Mostofi, J. Qiao, I. Souza, S. S. Tsirkin, J. R. Yates, and G. Pizzi, Wannier-function software ecosystem for materials simulations, Rev. Mod. Phys. **96**, 045008 (2024).

[68] D. N. Basov and T. Timusk, Electrodynamics of high-T_c superconductors, Rev. Mod. Phys. **77**, 721 (2005).

[69] D. N. Basov, R. D. Averitt, D. van der Marel, M. Dressel, and K. Haule, Electrodynamics of correlated electron materials, Rev. Mod. Phys. **83**, 471 (2011).

[70] H. Zhang, K. Haule, and D. Vanderbilt, Effective $J=1/2$ insulating state in Ruddlesden-Popper iridates: An LDA+DMFT study, Phys. Rev. Lett. **111**, 246402 (2013).

[71] P. Phillips, Colloquium: Identifying the propagating charge modes in doped Mott insulators, Rev. Mod. Phys. **82**, 1719 (2010).

[72] D. van der Marel and G. A. Sawatzky, Electron-electron interaction and localization in d and f transition metals, Phys. Rev. B **37**, 10674 (1988).

[73] K. Ueda, J. Fujioka, and Y. Tokura, Variation of optical conductivity spectra in the course of bandwidth-controlled metal-insulator transitions in pyrochlore iridates, Phys. Rev. B **93**, 245120 (2016).

[74] Y. Chen, Y.-H. Tian, R.-Q. He, and Z.-Y. Lu, Spin-orbit coupling effects on orbital-selective correlations in a three-orbital model, arXiv:2503.14435v1.

[75] R.-S. Li, R. Guo, Z. Xie, J.-T. Wang, and F. Wang, Spin-orbit-controlled correlation physics and orbital-selective electronic transitions in uranium monoxide revealed by many-body calculations, Phys. Chem. Chem. Phys. **27**, 15508 (2025).

[76] https://cstr.cn/31125.02.SHMFF.PPMS.

[77] https://cstr.cn/31125.02.SHMFF.